Translation reprogramming is an evolutionarily conserved driver of phenotypic plasticity and therapeutic resistance in melanoma

Paola Falletta,[1,10] Luis Sanchez-del-Campo,[1,10] Jagat Chauhan,[1] Maike Effern,[2] Amy Kenyon,[3] Christopher J. Kershaw,[4] Robert Siddaway,[1] Richard Lisle,[1] Rasmus Freter,[1] Matthew J. Daniels,[5] Xin Lu,[1] Thomas Tüting,[6] Mark Middleton,[7] Francesca M. Buffa,[7] Anne E. Willis,[8] Graham Pavitt,[4] Ze′ev A. Ronai,[9] Tatjana Sauka-Spengler,[3] Michael Hölzel,[2] and Colin R. Goding[1]

[1]Ludwig Institute for Cancer Research, Nuffield Department of Clinical Medicine, University of Oxford, Headington, Oxford OX3 7DQ, United Kingdom; [2]Department of Clinical Chemistry and Clinical Pharmacology, Unit for RNA Biology, University Hospital of Bonn, D-53127 Bonn, Germany; [3]Weatherall Institute of Molecular Medicine, Radcliffe Department of Medicine, University of Oxford, John Radcliffe Hospital, Headington, Oxford OX3 9DS, United Kingdom; [4]Division of Molecular and Cellular Function, School of Biological Sciences, Faculty of Biology, Medicine, and Health, The University of Manchester, Manchester M13 9PT, United Kingdom; [5]Division of Cardiovascular Medicine, Radcliffe Department of Medicine, University of Oxford, John Radcliffe Hospital, Headington, Oxford OX3 9DU, United Kingdom; [6]Laboratory of Experimental Dermatology, Department of Dermatology and Allergy, University Hospital Magdeburg, 39120 Magdeburg, Germany; [7]Department of Oncology, University of Oxford, Headington, Oxford OX3 7DQ, United Kingdom; [8]Medical Research Council Toxicology Unit, Leicester LE1 9HN, United Kingdom; [9]Tumour Initiation and Maintenance Program, Cancer Center, Sanford-Burnham Perbys Medical Discovery Institute, La Jolla, California 92037, USA

The intratumor microenvironment generates phenotypically distinct but interconvertible malignant cell subpopulations that fuel metastatic spread and therapeutic resistance. Whether different microenvironmental cues impose invasive or therapy-resistant phenotypes via a common mechanism is unknown. In melanoma, low expression of the lineage survival oncogene microphthalmia-associated transcription factor (MITF) correlates with invasion, senescence, and drug resistance. However, how *MITF* is suppressed in vivo and how MITF-low cells in tumors escape senescence are poorly understood. Here we show that microenvironmental cues, including inflammation-mediated resistance to adoptive T-cell immunotherapy, transcriptionally repress *MITF* via ATF4 in response to inhibition of translation initiation factor eIF2B. ATF4, a key transcription mediator of the integrated stress response, also activates *AXL* and suppresses senescence to impose the MITF-low/AXL-high drug-resistant phenotype observed in human tumors. However, unexpectedly, without translation reprogramming an ATF4-high/MITF-low state is insufficient to drive invasion. Importantly, translation reprogramming dramatically enhances tumorigenesis and is linked to a previously unexplained gene expression program associated with anti-PD-1 immunotherapy resistance. Since we show that inhibition of eIF2B also drives neural crest migration and yeast invasiveness, our results suggest that translation reprogramming, an evolutionarily conserved starvation response, has been hijacked by microenvironmental stress signals in melanoma to drive phenotypic plasticity and invasion and determine therapeutic outcome.

[*Keywords*: melanoma; phenotype-switching; invasiveness; MITF; TNFα]

Supplemental material is available for this article.

Received September 19, 2016; revised version accepted December 21, 2016.

Over many years, the genetic basis for cancer progression, including the development of drug resistance, has become increasingly well defined. However, superimposed on the heterogeneous genetic landscape within tumors is the influence of the intratumor microenvironment. Variations in a variety of microenvironmental cues, including

[10]These authors contributed equally to this work.
Corresponding author: colin.goding@ludwig.ox.ac.uk
Article published online ahead of print. Article and publication date are online at http://www.genesdev.org/cgi/doi/10.1101/gad.290940.116.

hypoxia, nutrient levels, signals from infiltrating immune cells, and the stroma, combine to impose specific gene expression programs that can determine invasive potential or therapeutic response. However, how drug-resistant and immunotherapy-resistant phenotypes relate to invasiveness and whether multiple intratumor microenvironmental cues converge on a "universal" regulator of phenotypic plasticity is poorly understood.

Melanoma, a cancer notorious for its ability to metastasize early, is an excellent model to dissect the complex relationship between invasion, drug resistance, and immunotherapy resistance. Gene expression profiling of 86 melanoma cell lines (Hoek et al. 2006) revealed that their gene expression signatures reflected one of two phenotypes: those that were invasive but poorly proliferative, or those that proliferated rapidly but were poorly invasive. The inverse correlation between invasive and proliferative signatures is not well understood but correlates with the expression of a key regulator of the melanocyte lineage, the microphthalmia-associated transcription factor (MITF) (Hodgkinson et al. 1993). MITF, a lineage survival oncogene (Garraway et al. 2005), drives proliferation (Carreira et al. 2006), promotes survival, and activates genes implicated in the differentiation-associated production of melanin. In contrast, MITF-low cells are slow-cycling and invasive (Carreira et al. 2006; Cheli et al. 2010). However, while short-term depletion of MITF leads to invasiveness and adoption of a tumor-initiating phenotype (Cheli et al. 2011b), longer-term MITF depletion leads to senescence (Giuliano et al. 2010). However, in vivo senescence is largely restricted to nevi (Michaloglou et al. 2005; Gray-Schopfer et al. 2006), although melanomas can contain many MITF-negative cells (Goodall et al. 2008; Riesenberg et al. 2015). How MITF is downregulated in vivo without provoking senescence is unknown, but low MITF is correlated with resistance to MEK and BRAF inhibitors (Konieczkowski et al. 2014; Muller et al. 2014; Dugo et al. 2015). Dissecting the molecular mechanisms underpinning the generation of MITF-low nonsenescent cells in vivo is therefore crucial to understanding the complex relationship between invasion, senescence bypass, and therapy resistance.

Here we show that MITF is translationally repressed by signals that trigger inhibition of the translation initiation factor eIF2B and transcriptionally repressed by ATF4, a translationally regulated transcription factor that is a key component of the integrated stress response (ISR). We reveal that translation reprogramming represents a master regulator of melanoma phenotypic plasticity that determines drug and immunotherapy resistance and metastatic potential.

Results

Glutamine limitation suppresses MITF

As an initial approach to understanding how the intratumor microenvironment might generate MITF-low cells, we focused on the potential role of glutamine. Glutamine, a conditionally essential amino acid, serves as a carbon and nitrogen source for anabolic metabolism and is commonly depleted in solid tumors (Roberts et al. 1956; Kamphorst et al. 2015). Although it can be synthesized de novo, many cells, especially cancer cells (Wise and Thompson 2010), including melanoma (Wang et al. 2014), require its exogenous supply, and glutamine is among one of five key amino acids depleted in melanoma tumor cores (Pan et al. 2016). Moreover, BRAF inhibitor-resistant melanomas exhibit a strong glutamine addiction (Hernandez-Davies et al. 2015; Baenke et al. 2016).

Transfer of melanoma cells from Dulbecco's modified Eagle medium (DMEM) to minimal essential medium (MEM) that lacks glutamine, serine, and glycine reduced MITF expression in human SKmel28, mouse B16 (Fig. 1A), or human IGR37 (Supplemental Fig. S1A) melanoma cell lines. MITF expression was restored upon addition of glutamine but not serine or glycine. Note that in most melanoma cell lines analyzed by Western blotting, MITF appears as two bands, the upper corresponding to MITF phosphorylation by ERK on Ser73 (Hemesath et al. 1998) that has been shown previously to increase binding to the p300 cofactor and enhance MITF's transcriptional activity (Price et al. 1998). The decrease in MITF on glutamine limitation was specific, as neither the PAX3 nor the BRN2 melanocyte lineage transcription factors were repressed (Fig. 1B). Transfer to MEM also triggered MITF phosphorylation (Fig. 1B) that was mediated by ERK, since it correlated with increased phospho-ERK (Supplemental Fig. S1B, left panel) and was blocked using the MEK inhibitor U0126 (Supplemental Fig. S1B, right panel). Importantly, glutamine titration (Fig. 1C) revealed that MITF expression was maintained in 2 mM glutamine compared with 4 mM glutamine in DMEM but was reduced in IGR37 cells at 0.5 mM glutamine, the physiological concentration of glutamine in blood. MITF expression was severely repressed in all cell lines at 0.1 mM glutamine.

A transient increase in MITF mRNA on glutamine starvation (Fig. 1D) correlated with increased phosphorylation of CREB (cyclic AMP response element-binding protein) (Fig. 1E), a well-known regulator of *MITF* expression (Bertolotto et al. 1996). Modification of CREB was inhibited by calmidazolium, a generic calmodulin antagonist (Supplemental Fig. S1C, top panels), or KN-93, a calcium-dependent calmodulin-dependent kinase II inhibitor (Supplemental Fig. S1C, bottom panels), consistent with CAMKII activation of CREB (Ma et al. 2014). Calmidazolium also blocked the early increase in MITF mRNA expression in response to glutamine deprivation (Supplemental Fig. S1D), consistent with CREB phosphorylation driving increased MITF promoter activity. H89, a cAMP-activated protein kinase A inhibitor, did not block CREB phosphorylation (data not shown). In summary, at early times, glutamine deprivation transiently increases MITF mRNA expression via Ca^{2+}-dependent CaMKII CREB phosphorylation, while ERK-mediated MITF phosphorylation will enhance its transcriptional activity (Price et al. 1998). However, the transition from acute to prolonged glutamine deprivation involves a dynamic regulation of MITF as it declines at later times.

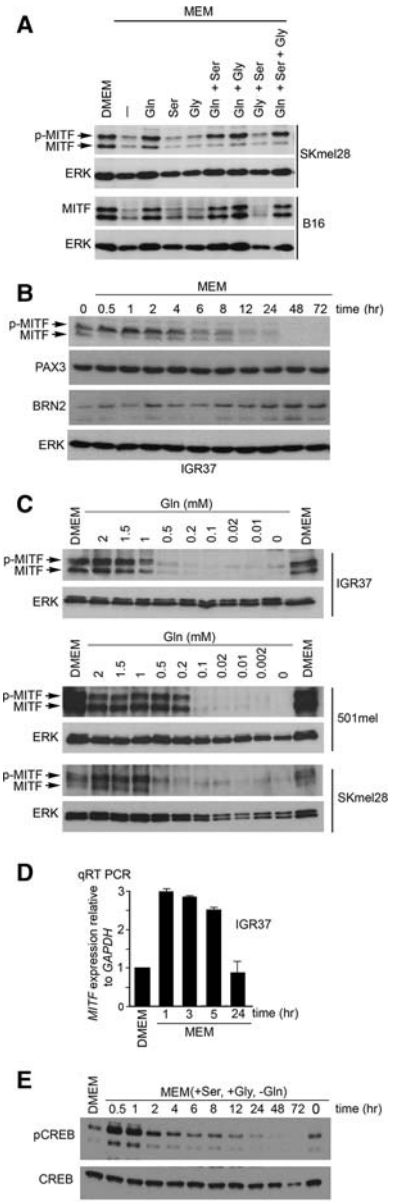

Figure 1. Glutamine limitation activates then suppresses MITF. (*A*) Western blot using anti-MITF cell lines grown in DMEM or MEM supplemented with the indicated amino acids. ERK was used as a loading control. (*B*) Western blot of IGR37 cells grown in DMEM ($t = 0$) or MEM. (*C*) Western blot of melanoma cells grown in DMEM or MEM supplemented with serine and glycine with the indicated concentrations of glutamine for 48 h. (*D*) Quantitative RT–PCR (qRT–PCR) using MITF-M-specific primers using mRNA from IGR37 cells grown in DMEM or MEM. (*E*) Western blot of IGR37 cells grown in DMEM or MEM supplemented with serine and glycine.

A transcription translation-coupled ATF4–MITF feedback loop

Using 19,982 probes for 16,118 genes, analysis of mRNA from IGR37 melanoma cells starved of glutamine for 6, 24, and 72 h revealed a total of 4336 differentially expressed genes (5003 probes) and confirmed MITF down-regulation (Supplemental Fig. S2A; Supplemental Table S1). Unsupervised hierarchical clustering of MITF-bound genes (Supplemental Fig. S2B; Supplemental Table S2; Strub et al. 2011) revealed clusters of coregulated genes (groups 1–7). Known MITF target genes, including many implicated in melanosome function (Fig. 2A) in group 6, were down-regulated, indicating that glutamine limitation promotes dedifferentiation. However, we observed no effect of glutamine deprivation on pigmentation, most likely because cells accumulated in G1 (see below) and consequently could not dilute pre-existing melanosomes through cell division.

Of the genes differentially regulated following glutamine starvation, one of the most interesting is *ATF4*. The ATF4 transcription factor is a key mediator of the ISR (Harding et al. 2003) and regulates genes that facilitate resolution of nutrient stress, for example, by up-regulating nutrient importers and genes implicated in autophagy. MITF phosphorylation correlated with increased mRNA encoding ATF4 (Fig. 2A; Supplemental Fig. S2C). As MITF directly regulated an ATF4 promoter luciferase reporter (Supplemental Fig. S2D) and bound the ATF4 promoter (Supplemental Fig. S2E), our results suggest that MITF activation may contribute to the ISR by up-regulating ATF4 at early times following glutamine starvation.

ATF4's translation is suppressed in nutrient-rich conditions but is increased when stress triggers phosphorylation of translation initiation factor eIF2α (Harding et al. 2003). Phosphorylation of eIF2α and ATF4 expression increased on glutamine starvation (Supplemental Fig. S2F), with p-eIF2α being detected prior to ATF4 accumulation (Fig. 2B). ATF4 expression was suppressed by glutamine but not serine or glycine (Supplemental Fig. S2G). Thapsigargin, a potent inducer of ER stress, was used as a positive control. ATF4 was induced and MITF was repressed at 0.2 mM glutamine (Supplemental Fig. S2H); at this concentration, glutamine induced ATF4 within 2 h and suppressed MITF by 24 h (Supplemental Fig. S2I).

Increased ATF4 on glutamine limitation correlated with regulation of its target genes (Fig. 2C; Supplemental Fig. S2J; Supplemental Table S3; Han et al. 2013) and decreased MITF mRNA (Fig. 2C). Notably, ATF4 suppressed MITF expression in three cell lines engineered to express doxycycline-inducible ATF4 in nutrient-rich conditions (Fig. 2D; Supplemental Fig. S2K) as well as *TYR* and *MART1* (Fig. 2D), MITF target genes involved in melanin production. Ectopic ATF4 expression also repressed an MITF promoter luciferase reporter (Fig. 2E), indicating that it likely has a direct effect on MITF transcription, and induced a G1 cell cycle arrest (Fig. 2F) similar to that mediated by MITF silencing (Carreira et al. 2006). However, while siRNA-mediated depletion of ATF4 largely abrogated the repression of MITF mRNA on glutamine starvation (Fig. 2G, left panel), repression of MITF protein expression was unaffected (Fig. 2G, right panel), indicating that MITF was repressed by a second ATF4-independent mechanism. This was most likely inhibition of MITF translation, since growth in MEM led to decreased

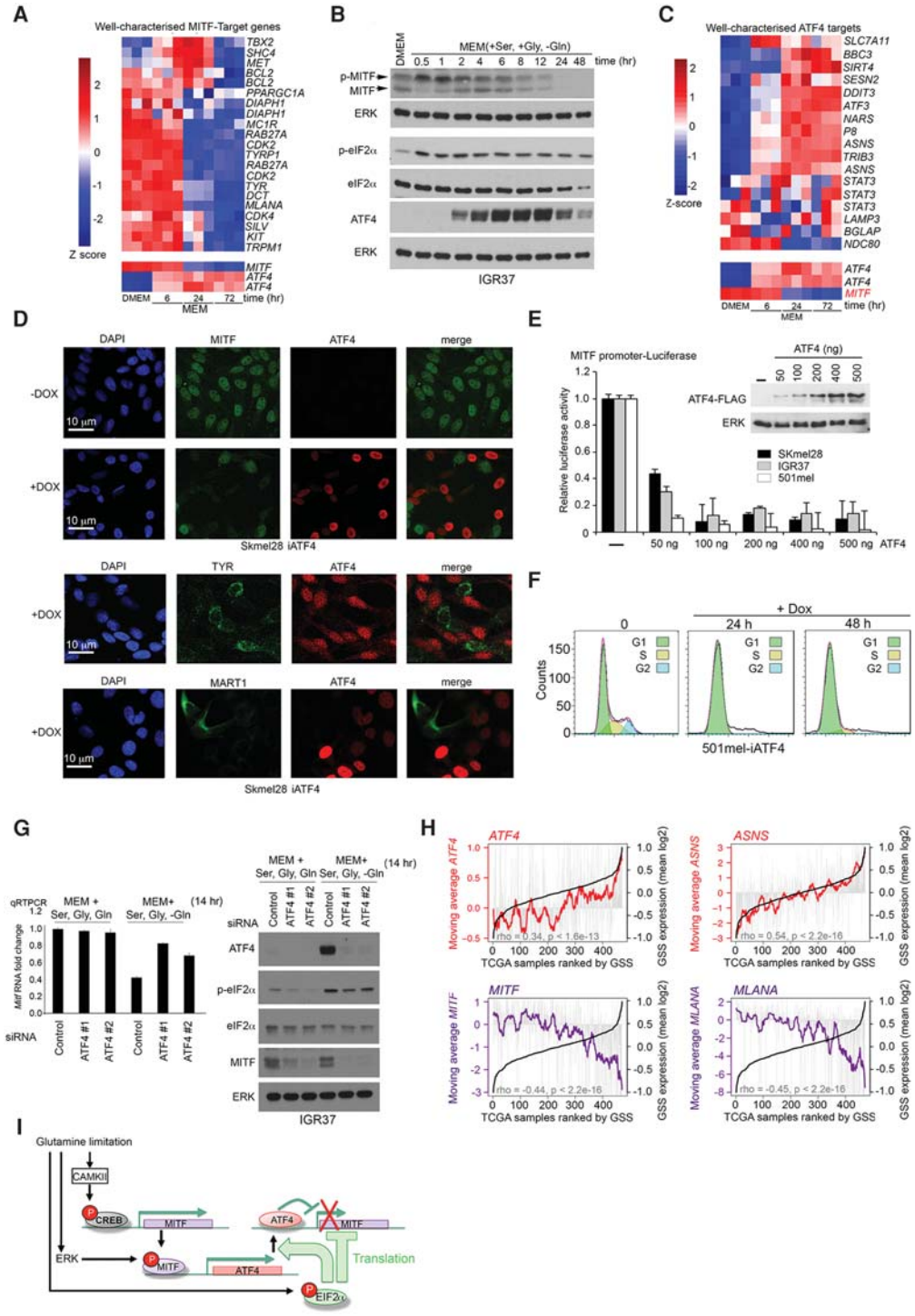

Figure 2. ATF4 couples MITF to the ISR. (*A*) Heat map from gene array data of well-characterized MITF targets from IGR37 cells grown in DMEM or MEM for the indicated times. (*B*) Western blot of IGR37 cells grown in DMEM or MEM supplemented with serine and glycine (–Gln). All samples are from the same experiment. (*C*) Heat map from gene array data of well-characterized ATF4 target genes. (*D*) Immunofluorescence using the indicated antibodies of SKmel28 cells expressing doxycycline-inducible ATF4 grown with or without 100 ng of doxycycline for 24 h. (*E*) Luciferase activity of an MITF promoter luciferase reporter cotransfected with an ATF4 expression vector. Results are expressed as average ± SD. $n = 3$. The *inset* shows a Western blot of ectopically expressed ATF4 with increasing amounts of transfected expression vector. (*F*) Flow cytometry profiles of iATF4 501mel cells before and after addition of doxycycline. (*G*) qRT–PCR of mRNA extracted from IGR37 cells grown with or without glutamine and exposed or not to anti-ATF4 siRNA (*left* panel) and a Western blot of the same cells (*right* panel). (*H*) Analysis of The Cancer Genome Atlas (TCGA) RNA sequencing (RNA-seq) data. The black line indicates TCGA samples ranked by average expression of a 103-gene glutamine starvation signature (GSS) score derived from the 6-h gene array time point (see Supplemental Table S4). Vertical gray lines indicate expression of the indicated gene in each melanoma sample. The colored line indicates the moving average of the indicated gene across 20 melanomas. (*I*) Model depicting early response to glutamine limitation.

^{35}S-methionine incorporation into protein (most likely owing to increased eIF2a phosphorylation) that was restored by addition of glutamine but not serine and glycine (Supplemental Fig. S2L, left panel). Immunoprecipitation of MITF revealed no ^{35}S-methionine incorporation into the protein unless glutamine was present. Coomassie staining was used as a control (Supplemental Fig. S2L, right panel). Collectively, these data suggest that MITF repression is likely mediated by both inhibition of its translation by p-eIF2α and repression of its transcription by ATF4. Overall, our results are consistent with translation reprogramming and induction of ATF4 coupling signals driving the ISR to melanoma dedifferentiation via repression of MITF.

We next derived a glutamine starvation signature (GSS) from 103 genes (Supplemental Table S4) whose expression is altered significantly after 6 h of glutamine deprivation. The 6-h time point was chosen to avoid potential indirect effects of glutamine limitation expected to occur at later times. The average expression of the GSS genes produced a score to rank 471 human melanomas characterized for gene expression in The Cancer Genome Atlas (TCGA; http://cancergenome.nih.gov). The expression of *ATF4* and its target, *ASNS*, followed the GSS ranking (Fig. 2H, top panels); melanomas with a low GSS score exhibited an average low *ATF4*/*ASNS* expression, and those with a high GSS score displayed higher *ATF4*/*ASNS* expression. In contrast, expression of *MITF* or its differentiation-associated target, *MLANA*, was inversely correlated with the GSS score (Fig. 2H, bottom panels). Mechanistically, glutamine limitation initiates a transcription/translation-coupled feedback loop in which MITF first increases ATF4 mRNA, eIF2α phosphorylation promotes ATF4 translation, and ATF4 represses *MITF* transcriptionally, while MITF translation is also blocked, most likely as a consequence of p-eIF2α-mediated inhibition of eIF2B (Fig. 2I). siRNA-mediated depletion of MITF initially drives invasiveness (Carreira et al. 2006) and subsequently senescence (Giuliano et al. 2010), yet, paradoxically, melanomas contain nonsenescent MITF-negative cells. We reasoned that siMITF-induced senescence might be circumvented if MITF were silenced via a physiological mechanism, such as by translation reprogramming and ATF4. Consistent with this, siMITF induces senescence detected using senescence-associated-β-galactosidase (SA-β-gal) activity (Fig. 3A, top panels; Supplemental Fig. 3A), whereas, in contrast, depletion of glutamine that silences MITF expression (Fig. 1) did not lead to senescence (Fig. 3A, bottom panels; Supplemental Fig. S3A). Glutamine-deprived cells exhibited reduced S phase and accumulated in G1 (Fig. 3B), but, unlike senescence, the cell cycle arrest was reversible, and cells re-entered the cell cycle on glutamine refeeding (Fig. 3B); even after 17 d of glutamine starvation, refeeding with glutamine reversed the loss of MITF and its differentiation-associated target, MLANA (Fig. 3C). Significantly, induction of ATF4 in nutrient-rich medium was sufficient to suppress siMITF-induced senescence (Fig. 3D). MITF-low nonsenescent cells observed in tumors can therefore be generated by signals that promote increased ATF4 translation.

An ATF4-high/MITF-low state is insufficient to drive invasiveness

The GSS correlated with two independent melanoma invasiveness signatures (Hoek et al. 2006; Verfaillie et al. 2015) in the TCGA human melanoma cohort (Fig. 3E; Supplemental Table S4). The GSS correlated even better with the Verfaillie invasive signature in a recent patient-derived single-cell melanoma RNA sequencing (RNA-seq) data set (Tirosh et al. 2016), suggesting that much of the noise in the correlation with the TCGA data set arises from nonmelanoma cells within the tumor. Note that the overlap between the GSS and the Hoek and Verfaillie signatures is small, and the correlation could be recapitulated even without the overlapping genes (data not shown). The GSS also correlates with the Verfaillie invasiveness signature in independent cohorts of melanoma cell lines (Broad [Lin et al. 2008], Queensland [Johannessen et al. 2013], and Duke [Augustine et al. 2009]) (Supplemental Fig. S3B, left panels) and their invasiveness (Supplemental Fig. S3B, right panel; Widmer et al. 2012). Glutamine limitation promoted invasiveness (Fig. 3F) and up-regulated mRNAs encoding the epithelial-to-mesenchyme transition (EMT)-associated transcription factor ZEB1, CDH2 (N-cadherin), and FN1 (Fibronectin 1) (Supplemental Fig. S3C). This observation was corroborated by examining EMT-associated gene expression in the gene array data derived from glutamine-depleted cells (Supplemental Table S1). The observed up-regulation of ZEB1 and down-regulation of SNAI2 are hallmarks of reprogramming by EMT-associated transcription factors in late-stage melanoma (Caramel et al. 2013). siRNA-mediated depletion of MITF triggers invasion (Carreira et al. 2006), and low MITF in vivo and in vitro correlates with invasiveness. We therefore expected ATF4-mediated repression of MITF to promote a proliferative-to-invasive phenotype switch. Surprisingly, however, ATF4 induction in nutrient-rich medium (Fig. 3F, right) efficiently silenced MITF (Fig. 2D) but consistently failed to promote invasion. Since an ATF4-high/MITF-low state more accurately reflects the in vivo setting than siRNA depletion, we reassessed MITF's role in melanoma progression. Notably, while some cells die under glutamine limitation, death was substantially increased on doxycycline-mediated induction of MITF in the iMITF 501mel cell line (Fig. 3G). Most likely this is because MITF promotes proliferation, for example, by activating CDK expression (Du et al. 2004) to impose a high-nutrient-demand state incompatible with nutrient limitation. Surprisingly, therefore, an ATF4-high/MITF-low state is insufficient to establish an invasive phenotype. This result was further substantiated by examining the effect of glutamine deprivation on invasiveness in a panel of cell lines with different levels of MITF. In all cases, with the exception of the MITF-negative IGR39 cell line, glutamine deprivation led to transient activation of ATF4 expression and increased invasiveness irrespective of MITF status (Fig. 3H). Understanding the different response of the IGR39 cells will require further investigation.

Inhibition of eIF2B drives invasiveness

If ATF4-mediated repression of MITF is insufficient to initiate invasiveness, as expected, what is? Nutrient limitation increases ATF4 expression but also leads to global reprogramming of translation via p-eIF2α-mediated inhibition of eIF2B. However, when ATF4 is induced by doxycycline in nutrient-rich conditions to repress MITF, translation reprogramming would not occur. In breast cancer activation of PERK, an eIF2α kinase has been reported to lie downstream from EMT (Feng et al. 2014). In contrast, our results suggest that invasiveness occurs as a consequence of eIF2α phosphorylation. To define the role of p-eIF2α in invasiveness and uncouple its activation from upstream signals, we treated cells with salubrinal, a selective inhibitor of eIF2α dephosphorylation (Boyce et al. 2005). As expected, salubrinal increased ATF4 and decreased MITF expression (Fig. 4A; Supplemental Fig. S4A) but also down-regulated E-cadherin (Supplemental Fig. S4B) and induced invasiveness (Fig. 4B). Significantly, the ISR inhibitor ISRIB, a drug that stabilizes eIF2B dimers to render cells insensitive to eIF2α phosphorylation (Sidrauski et al. 2015), prevented invasiveness arising from glutamine limitation (Fig. 4C). Using a panel of melanoma lines with different MITF levels and driver mutation statuses, we observed that neither salubrinal nor ISRIB caused any significant cell death (Supplemental Fig. S4C) and that, while NRAS mutant lines appeared less susceptible to death on glutamine deprivation, more extensive analysis will be required to determine whether this is significant. To confirm the role of eIF2α phosphorylation in invasion, we stably expressed Flag-tagged eIF2α wild type and an S51A mutant that acts as a dominant negative in 501mel cells and examined their response to glutamine limitation. The results revealed that while cells expressing ectopic wild-type eIF2α induced ATF4 (Fig. 4D) and became invasive (Fig. 4E), those expressing the dominant-negative eIF2α S51A

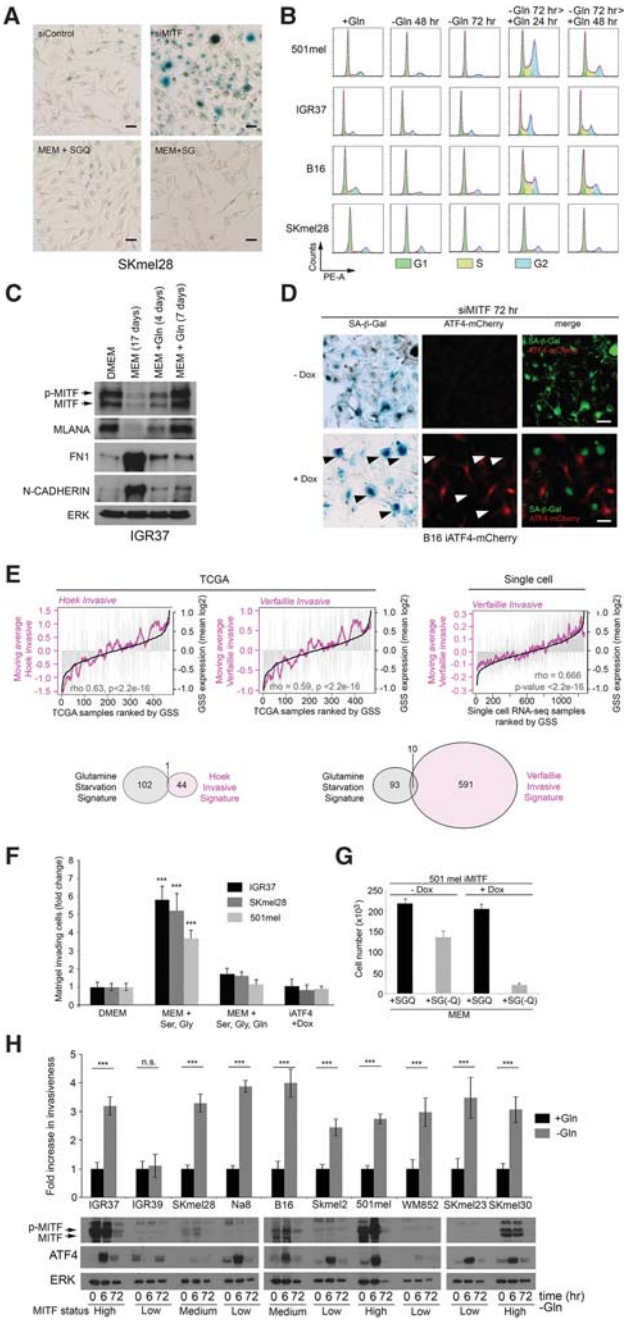

Figure 3. Glutamine limitation drives ATF4-mediated senescence bypass and invasiveness. (*A*) SA-β-gal activity in SKmel28 cells grown in DMEM and depleted for MITF or in MEM supplemented with serine (S) and glycine (G) or glutamine (Q) as indicated. Bars, 10 µm. (*B*) Flow cytometry of the indicated melanoma cell lines grown in the presence or absence of glutamine as indicated. (*C*) Western blot using the indicated antibodies of IGR37 cells depleted for glutamine and refed as indicated. (*D*) SA-β-gal activity in B16 cells expressing doxycycline-inducible ATF4 and mCherry. Cells were depleted for MITF using siRNA, and, 24 h later, ATF4 was induced using 100 ng of doxycycline. SA-β-gal is false-colored green to facilitate visualization of colocalization. Arrowheads indicate SA-β-gal-positive cells not expressing ATF4. Bars, 10 µm. (*E*) Analysis of TCGA human melanoma samples or melanoma single-cell RNA-seq data (Tirosh et al. 2016) for the presence of the Hoek (Hoek et al. 2006) or Verfallie (Verfaillie et al. 2015) invasiveness signature in samples ranked by the GSS score. Vertical gray lines indicate expression of the invasive signatures in each melanoma sample. Colored line indicates the moving average of the invasive signature across 20 melanoma samples. Venn diagrams indicate the number of genes in each signature (see also Supplemental Table S4). (*F*) Matrigel invasiveness assay in melanoma cells grown in DMEM or MEM supplemented with serine, glycine, or glutamine or the same cell lines expressing doxycycline-inducible ATF4. Results are expressed as mean ± SD of at least three biological replicates. (***) $P = <0.001$. (*G*) Cell numbers in an iMITF 501mel cell line grown in the presence or absence of doxycyline or minus glutamine as indicated. Results are expressed as mean ± SD of three biological replicates. (*H*, *top* panel) Matrigel invasiveness assays using the indicated cell lines grown with or without glutamine deprivation for 72 h as indicated. Results are expressed as mean ± SD of three biological replicates. (***) $P = <0.001$. (*Bottom* panel) Western blot at the indicated times of cell lines grown in the presence or absence of glutamine as indicated.

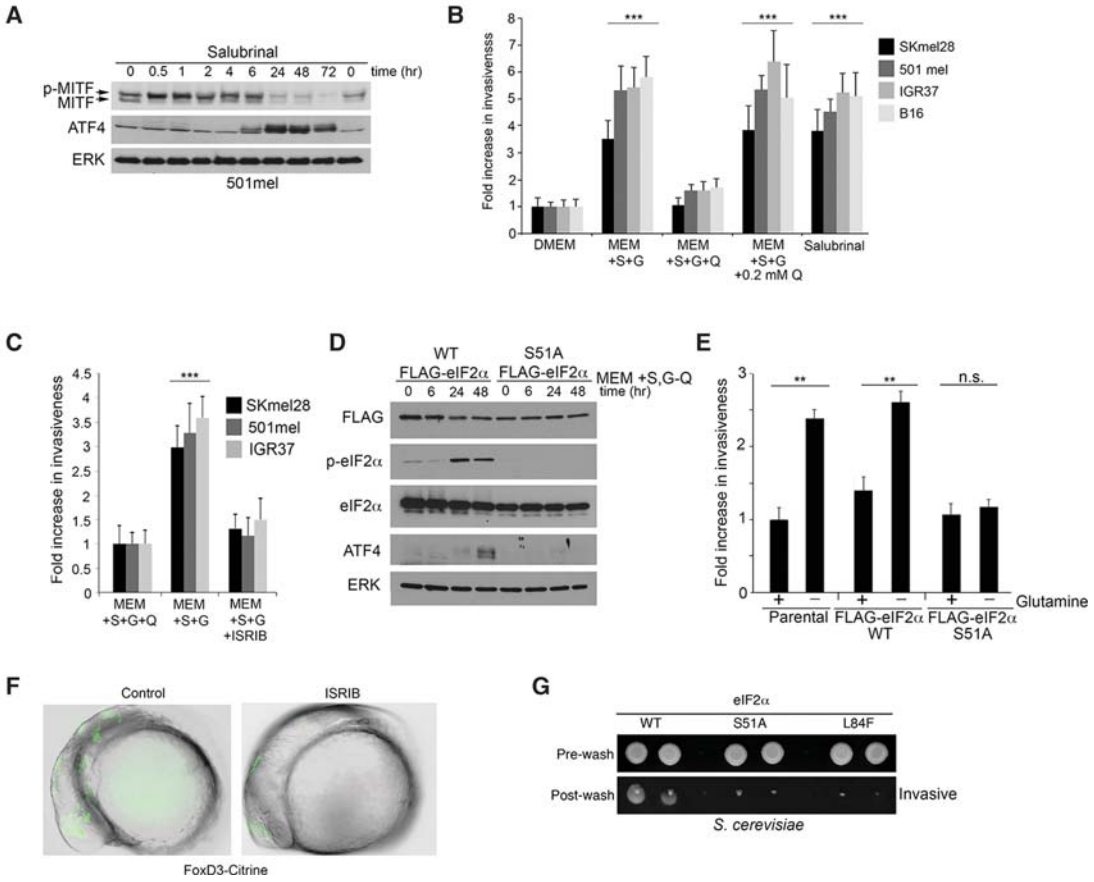

Figure 4. Inhibition of eIF2B drives invasion. (*A*) Western blot of 501mel cells grown in DMEM and treated with 20 µM salubrinal. (*B*) Matrigel invasion assays for cells grown in DMEM; MEM; MEM supplemented with serine (S), glycine (G), or glutamine (Q); or DMEM plus 20 µM salubrinal as indicated. Statistical analysis used a Student's unpaired *t*-test assuming equal variances. Data are presented as mean ± SD of at least three biological replicates. (***) $P = <0.001$. (*C*) Matrigel invasion assays for cell lines grown in DMEM, MEM, or MEM supplemented with serine (S) and glycine (G) (−Gln) in the presence or absence of 10 µM ISRIB. Results are expressed as mean ± SD of at least three biological replicates. (***) $P = <0.001$. (*D*) Western blot using the indicated antibodies of 501mel cells stably expressing Flag-tagged wild-type or S51A mutant eIF2α and starved of glutamine for the indicated times. (*E*) Matrigel invasion assays for parental 501mel cells or derivatives stably expressing Flag-tagged wild-type or S51A mutant eIF2α grown in the presence or absence of glutamine. Results are expressed as mean ± SD of at least three biological replicates. (**) $P = <0.01$; (n.s.) not significant. (*F*) Zebrafish embryo expressing Foxd3-citrine in the neural crest 5 d after fertilization with or without 10 µM ISRIB. (*G*) Yeast invasion assay showing wild-type and mutant colonies grown on YPD agar before and after washing.

mutant failed to do either. Collectively, these data firmly place inhibition of eIF2B as a crucial driver of melanoma invasiveness. Significantly, this pathway is also activated by nelfinavir (Supplemental Fig. S4D), a drug recently proposed as a melanoma therapeutic (Smith et al. 2016), raising the possibility that cells exposed to sublethal concentrations of nelfinavir in vivo may become more invasive.

Since melanomas arise from melanocytes that have their developmental origins in the migrating neural crest, we asked whether ISRIB would also block neural crest migration. Using zebrafish in which neural crest cells are fluorescently tagged, migration was readily observed in untreated embryos, but, in ISRIB-treated fish, neural crest cells were maintained on the midline (Fig. 4F). Although we were unable to confirm the effect of ISRIB on ATF4, MITF, and eIF2α in the fish neural crest owing to the absence of antibodies that recognize these factors in fish, this result nevertheless suggests that translation reprogramming imposed by signals originating in the neural crest converge on inhibition of eIF2B, in effect hijacking the starvation response to promote migration.

To provide genetic evidence for a role of translation reprogramming as an evolutionarily conserved driver of invasive behavior, we also tested whether inhibition of eIF2B is required for invasion in yeast. Under nutritional stress, the budding yeast *Saccharomyces cerevisiae* form invasive chains to adopt a filamentous growth phenotype (Gimeno et al. 1992). Yeast bearing a wild-type eIF2α gene, an S51A mutant, or an L84F mutant that permits eIF2α-S51 phosphorylation but prevents interaction with eIF2B were grown on agar. After washing with water, only cells that invaded the substrate were retained. This assay revealed that cells with wild-type eIF2α are invasive,

whereas yeast bearing either the eIF2α S51A or L84F mutation are not (Fig. 4G). This genetic evidence strongly supports our contention that migration/invasiveness is an evolutionarily conserved response to inhibition of eIF2B and consequent translation reprogramming. Moreover, since yeast do not have an MITF gene, the result again underscores our observation above (Fig. 3F,H) that invasion can be uncoupled from effects on MITF expression.

Tumor necrosis factor α (TNFα) mediates translation reprogramming, ATF4 expression, and repression of MITF

Given that invasiveness in yeast, neural crest, and melanoma is imposed via inhibition of eIF2B, we predicted that other intratumor microenvironmental signals would hijack this evolutionarily conserved starvation response to impose invasiveness via the same mechanism even in nutrient-rich conditions. Inflammatory cytokines originating from infiltrating immune cells play a critical role in tumor evolution. Of these, one of the more important is TNFα. Smith et al. (2014) reported that TNFα promotes melanoma growth and therapeutic resistance by up-regulating MITF, which should promote differentiation. In contrast, other studies report that TNFα down-regulates MITF (Landsberg et al. 2012; Konieczkowski et al. 2014; Riesenberg et al. 2015), decreases differentiation, and promotes a slow-cycling phenotype (Ostyn et al. 2014), a characteristic of MITF-low cells (Cheli et al. 2011b). Significantly, a recently described melanoma TNFα response gene set (Riesenberg et al. 2015) positively correlated with the GSS score in the TCGA melanoma cohort as well as the single-cell RNA-seq patient-derived melanoma data from Tirosh et al. (2016) (Fig. 5A). The overlap between the two signatures was small, and the correlation could be recapitulated even without the overlapping genes (data not shown). This suggests that the responses to glutamine starvation and TNFα converge on a common melanoma phenotype. In culture, although the response was variable between cell lines, TNFα initiated a response remarkably similar to that observed on glutamine limitation (Fig. 5B); any increase in MITF, as observed by Smith et al. (2014), was transient, and, in all cell lines, TNFα ultimately promoted ATF4 expression (indicative of p-eIF2α-mediated translation reprogramming) and invasiveness (Fig. 5C) that would be consistent with TNFα driving an MITF-low phenotype and dedifferentiation.

To explore further the convergence of inflammatory, invasive, and glutamine starvation gene expression programs in vivo, we used gene expression data from a mouse model of inflammation-mediated melanoma dedifferentiation (Fig. 5D, left; Landsberg et al. 2012). In this model, tumors initially respond to adoptive cell transfer therapy using transgenic cytotoxic pmel-1 T cells targeting the melanoma differentiation antigen gp100 (also known as Pmel). However, TNFα and other cytokines released from the T cells and tumor-infiltrating myeloid immune cells dedifferentiate melanoma cells in vivo, leading to depigmentation, gp100 antigen down-regulation, and escape from pmel-1 T-cell immunotherapy. The HCmel3 mouse melanoma cell line used also responds to glutamine deprivation and/or TNFα exposure by down-regulating MITF (Fig. 5D, right). Gene set enrichment analysis (GSEA) (Fig. 5E) of the gene expression profile from the inflammation-driven dedifferentiated relapsed melanomas revealed a strong positive correlation to TNFα response genes and the Hoek and Verfaillie invasive gene sets, consistent with TNFα-mediated dedifferentiation driving proinvasive phenotype switching. Significantly, the in vivo gene expression data also revealed a strong positive correlation with the GSS, and relapsed tumors were strongly depleted for both the Hoek and Verfaillie proliferative gene expression signatures (Fig. 5E; Supplemental Table S4). Moreover, expression of *Mitf* and its target, *Mlana*, were robustly down-regulated in the relapsed tumors, whereas *Atf4* and *Asns* were strongly up-regulated (Fig. 5F). Although we did not show that there is a causative relationship between translation reprogramming and resistance to pmel adoptive T-cell therapy in vivo, collectively, these data are consistent with an in vivo inflammation-mediated dedifferentiation phenotype switch associated with adoptive T-cell therapy ultimately arising through a stress response related to that observed on glutamine deprivation.

ATF4 drives the MITF-low/AXL-high drug resistance signature

Strikingly, the relapsed murine tumors also exhibited strong up-regulation of the AXL receptor tyrosine kinase (Fig. 5F); an MITF-low/AXL-high phenotype (Supplemental Fig. S4E) is a well-characterized hallmark of BRAF inhibitor resistance in human melanoma (Konieczkowski et al. 2014; Muller et al. 2014; Dugo et al. 2015; Tirosh et al. 2016) and has been linked to resistance to anti-PI3K therapy in head and neck cancer (Elkabets et al. 2015). How AXL expression is up-regulated is not well established. However, AXL levels correlated with the GSS score in TCGA melanoma samples (Fig. 6A, left), and a 100-gene AXL program signature (Supplemental Table S4; Tirosh et al. 2016) also closely correlated with the GSS in the single-cell melanoma gene expression profile from Tirosh et al. (2016) (Fig. 6A, right). Significantly, glutamine depletion (Fig. 6B,C) or doxycycline-mediated induction of ATF4 in nutrient-rich medium (Fig. 6D; Supplemental Fig. S4F) imposed an MITF-low/AXL-high state, suggesting that stresses driving ATF4 protein expression within tumors may initiate the observed MITF-low/AXL-high phenotype.

Inhibition of eIF2B correlates with the IPRES (innate anti-PD-1 resistance) gene expression signature

Interaction between T-cell-associated PD-1 and its ligand, PD-L1 (PD-1), dampens T-effector function and protects melanomas from immune rejection. Consequently, blockade of the PD-1/PD-L1 axis can provide a major therapeutic benefit (Wolchok et al. 2013). However, nonresponsiveness to anti-PD-1 therapy is associated with a characteristic gene expression pattern that also includes elevated AXL expression, termed the IPRES signature

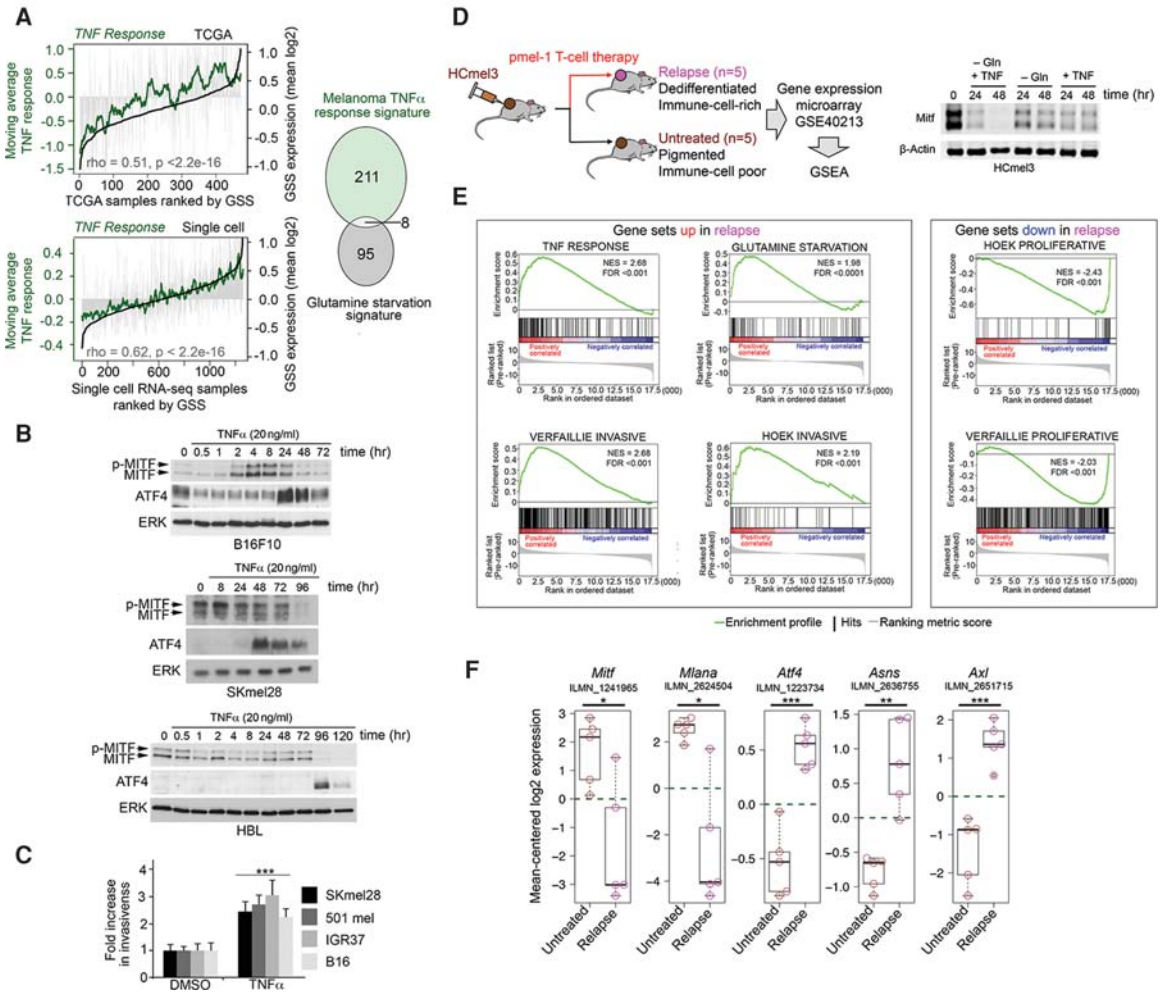

Figure 5. TNFα activates ATF4 to trigger a GSS. (*A*) Analysis of TCGA or single-cell (Tirosh et al. 2016) human melanoma samples for the presence of a 219-gene TNFα response signature (see also Supplemental Table S4; Landsberg et al. 2012) in samples ranked by the GSS score (black line). Vertical gray lines indicate expression of the TNFα signature in each melanoma sample. The colored line indicates the moving average of the TNFα signature across 20 melanoma samples. The Venn diagram indicates the number of genes in each signature. (*B*) Western blot of melanoma cells treated with 20 ng/mL TNFα. (*C*) Matrigel invasiveness assay in melanoma cells grown in DMEM with 20 ng/mL TNFα. Statistical analysis was carried out using Student's unpaired *t*-test assuming equal variances. Data are presented as mean ± SD of at least three biological replicates. (***) $P = <0.001$. (*D*) Strategy for analysis of pmel adoptive T-cell therapy-mediated dedifferentiation and relapse of mouse melanoma (*left*) and Western blot (*right*) of murine melanoma Hcmel3 cells grown in the presence or absence of TNFα or glutamine. (*E*) Gene set enrichment analysis (GSEA) of gene array data derived from relapsed mouse melanomas. (NES) Normalized enrichment score; (FDR) false discovery rate. (*F*) Box plots showing the relative expression of the indicated genes from gene arrays of untreated or relapsed mouse melanomas after T-cell immunotherapy. The respective gene probe identities are indicated *below* the gene symbols. Box plot horizontal lines and whiskers indicate quartiles. (*) $P < 0.05$; (**) $P < 0.01$; (***) $P < 0.001$, unpaired two-sided *t*-test.

(Hugo et al. 2016). Although the IPRES signature is found in a major subset of nonresponsive tumors, how it is established is unknown. Since AXL expression is associated with poor response to anti-PD-1 therapy (Hugo et al. 2016) and is induced by ATF4, we asked whether the IPRES gene expression signature correlated with the GSS score in the TCGA melanoma cohort. Using gene set variation analysis (GSVA) to compare the IPRES signature in the top and bottom 75 melanomas ranked by the GSS revealed a very strong correlation (Fig. 6E). Importantly, we saw a similar enrichment using a gene expression signature derived from cells treated for 24 h with salubrinal (Supplemental Tables S4, S5) that inhibits eIF2B by promoting eIF2α phosphorylation. Thus, translation reprogramming not only is associated with invasiveness, dedifferentiation, and resistance to adoptive T-cell therapy but can also impose a gene expression program that predicts poor response to anti-PD-1 immunotherapy.

Translation reprogramming promotes tumor colonization

Rare, stochastically occurring, slow-cycling MITF-low cells exhibit increased tumor initiation capacity (Cheli

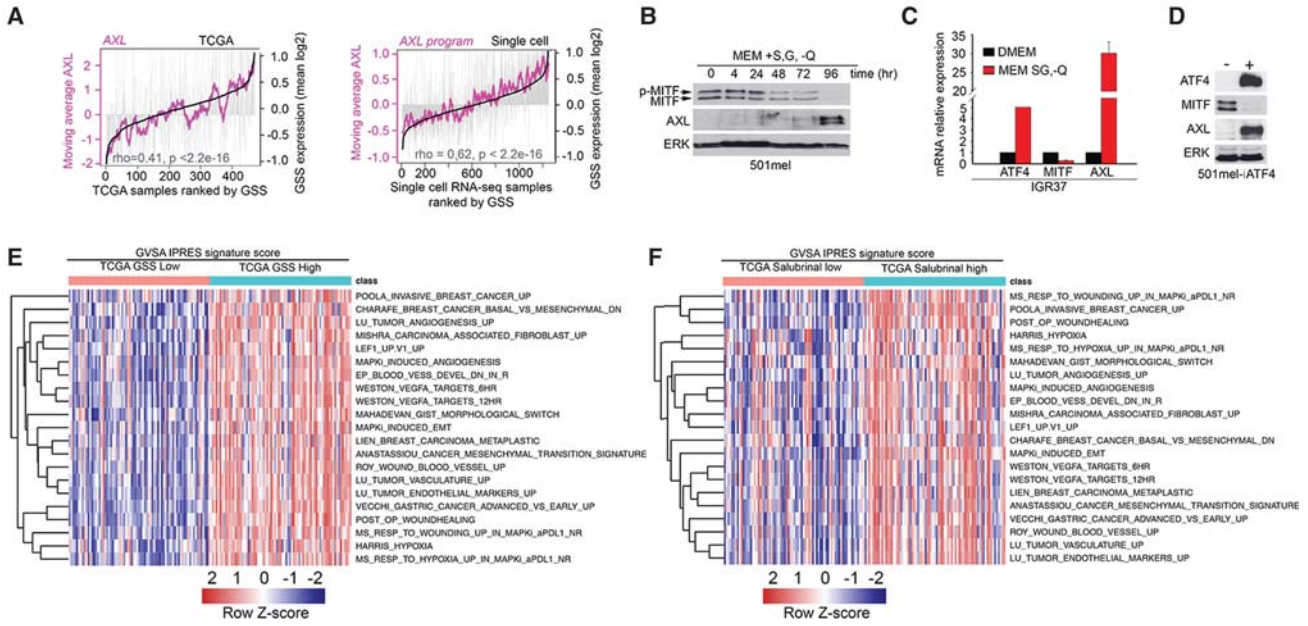

Figure 6. Translation reprogramming is sufficient to trigger melanoma invasiveness and drives therapeutic resistance signatures. (*A*) Analysis of TCGA human melanoma samples ranked by the GSS score (black line) for AXL expression or single-cell melanoma for an AXL signature. Gray lines indicate the expression of AXL in each melanoma sample. The colored line indicates the moving average of AXL or AXL signature expression across 20 melanoma samples. (*B*) Western blot of 501mel cells grown in DMEM or MEM supplemented with serine (S) and glycine (G) minus Gln (Q) for the indicated times. (*C*) qRT–PCR of mRNA from IGR37 cells grown in DMEM or MEM supplemented with serine (S) and glycine (G) minus Gln (Q) for 48 h. (*D*) Western blot of 501mel cells grown in DMEM inducibly expressing ATF4 for 24 h in response to 100 ng of doxycycline. (*E*,*F*) Heat maps showing gene set variation analysis (GSVA) scores of the IPRES (innate anti-PD-1 resistance) gene signatures enriched in the top and bottom 75 TCGA melanoma samples ranked by the GSS (*E*) or salubrinal (*F*) signatures (see also Supplemental Table S4).

et al. 2011b). However, how such cells are generated in vivo is poorly understood. Since glutamine deprivation produces MITF-low cells, it was possible that translation reprogramming controls tumor initiation capacity. We therefore injected B16 melanoma cells into the tail vein of immunocompetent C57/Bl6 mice and assessed tumor formation in the lungs, an assay that measures the capacity to survive in the circulation as well as providing a quantitative measure of tumor-initiating capacity. After 20 d, a few small tumors were visible in the lungs (Fig. 7A), consistent with the presence of infrequent MITF-low tumor-initiating cells (Cheli et al. 2011b). In contrast, B16 cells deprived of glutamine prior to injection led to a massive tumor burden. Since inhibition of eIF2B is sufficient to increase invasiveness, we compared the effects of salubrinal with glutamine deprivation in the tail vein injection assay. Mice were examined 15 d following injection, when tumors from untreated B16 cells were barely visible (Fig. 7B). In contrast, many pigmented tumors were readily visible in mice injected with either glutamine-deprived or salubrinal-treated cells, indicating that inhibition of eIF2B increases tumor initiation capacity in this assay.

Discussion

Given the role of MITF in integrating so many aspects of melanoma biology and the fact that an MITF-low state correlates with drug resistance, understanding how the tumor microenvironment impacts on MITF expression is key to the development of effective anti-melanoma therapies. Here we reveal a crucial and previously unsuspected link between the ISR and the gene expression programs underpinning melanoma biology regulated by MITF; microenvironmental signals, including glutamine limitation and TNFα, converge to inhibit eIF2B, leading to a block in MITF translation as well as ATF4 expression and direct repression of MITF transcription. Although we did not examine the molecular mechanism underpinning repression of *MITF* by ATF4, it is likely that it occurs either by displacement of the MITF promoter activator CREB that shares a related DNA-binding motif or via recruitment of a repressive cofactor, as has been observed at the *Apelin* gene promoter (Jeong et al. 2014).

The role of ATF4 and translation reprogramming in resistance to adoptive T-cell therapy is clinically relevant. Anti-PD1 or PD-L1 therapy is not effective in a significant proportion of patients, resistance is an increasing issue, and there are continuing efforts to enhance adoptive T-cell therapy or develop anti-melanoma vaccines that work via activation of T cells. Identifying the potential mechanisms of resistance, such as inflammation-mediated inhibition of differentiation via ATF4 and translation-mediated repression of MITF, provides opportunities to target translation reprogramming and restore sensitivity to T-cell-mediated therapies. Moreover, although we did

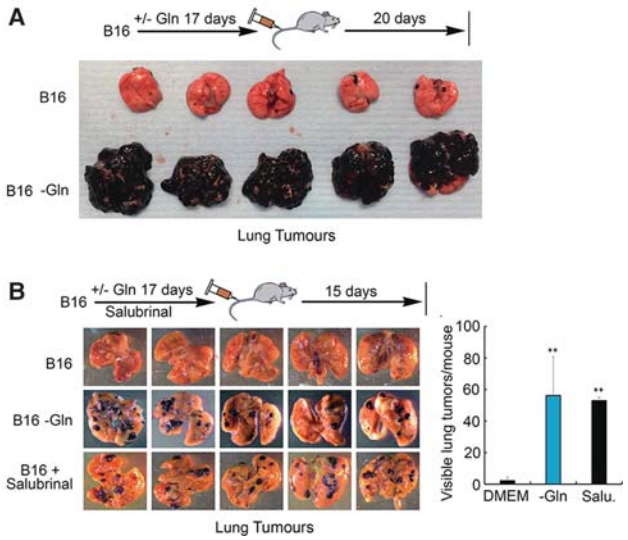

Figure 7. Translation reprogramming enriches for tumor initiation capacity. (*A*) Lung colonization by B16 melanoma cells grown in DMEM or for 17 d in MEM prior to tail vein injection. Mice were sacrificed 20 d after injection. (*B*) Lung colonization by B16 melanoma cells grown in DMEM or for 17 d in MEM supplemented with serine and glycine (−Gln) or in DMEM plus 20 µM salubrinal prior to tail vein injection. Mice were sacrificed at 15 d after injection. Quantification was made by counting visible tumors using a dissecting microscope. Error bars indicate mean ± SD. $n = 5$. (**) $P = <0.01$.

not show a direct effect on the interaction between the immune system and melanoma cells, both glutamine starvation and salubrinal treatment generate a gene expression signature that can predict the presence of an established signature (IPRES) (Hugo et al. 2016) of immunotherapy resistance. This raises the possibility that translation reprogramming may play a key role in modulating the interaction between melanoma cells and the immune system in response to microenvironmental cues, although further work will be required to determine exactly how this might be achieved. Importantly, ATF4 expression can also drive the previously unexplained MITF-low/AXL-high gene expression program (Konieczkowski et al. 2014; Muller et al. 2014; Dugo et al. 2015) that is a hallmark of BRAF inhibitor resistance.

In addition to being correlated with drug resistance, MITF-low cells are invasive. One conclusion from previous studies has been that invasion and proliferation are inversely correlated (Hoek et al. 2006) and that MITF somehow suppresses invasiveness. Why invasion and proliferation are inversely correlated and how MITF might block invasion have not been established previously. Our results provide an explanation. Inhibition of eIF2B in response to signals, including nutrient deprivation, inflammation, and other upstream stresses, enables cells to mount a two-armed adaptive response: First, inhibition of eIF2B reduces nutrient demand by decreasing the majority of translation that is necessary for proliferation. Second, cells increase ATF4 transcription via MITF and enhance translation of ATF4 that can drive amino acid import and autophagy to increase nutrient supply. Supply can be further increased via translation reprogramming-mediated invasiveness that would enable cells to escape the stress and seek new sources of nutrients. Consequently, there is an inverse correlation between proliferation and invasiveness, in which global translation is curtailed.

We also show that induction of ATF4 to reduce MITF mRNA expression in nutrient-rich conditions can generate an ATF4-high/MITF-low nonsenescent state as observed in tumors but that, surprisingly, this is insufficient to promote invasion. Together with our observation that maintenance of MITF expression in glutamine-limited conditions is incompatible with survival, we suggest that the ability of MITF to promote proliferation, a high-nutrient-demand state, is incompatible with nutrient limitation; it is translation reprogramming mediated by inhibition of eIF2B rather than reduced MITF expression or high ATF4 that is key to driving invasiveness, but MITF expression must be decreased to permit survival. This explains why therapeutic strategies that increase MITF expression, such as the use of methotrexate, can be highly effective at preventing metastatic spread (Saez-Ayala et al. 2013). More importantly, our discovery that translation reprogramming can repress MITF has significant implications for therapeutic use of drugs that deliberately (Cerezo et al. 2016) or inadvertently up-regulate ER stress and ATF4 in melanoma. Nelfinavir, identified recently in a drug-repurposing screen as a melanoma therapeutic that down-regulates MITF (Smith et al. 2016), is known to inhibit an eIF2α phosphatase (De Gassart et al. 2016), and, while reported to down-regulate MITF via suppression of PAX3, we show that nelfinavir can also promote translation reprogramming and ATF4 expression in melanoma. We suggest that, although down-regulation of MITF via stress-induced translation of ATF4 may have therapeutic advantages in some settings where cells may be susceptible to dynamic changes in MITF expression, there is a danger that suppression of MITF via drugs that promote translation reprogramming will increase metastatic spread at sublethal doses likely to encountered by many cells in vivo.

Although we focused here on the generation of MITF-low nonsenescent melanoma cells via ATF4 and phosphorylation of eIF2α, it is also clear that other factors can transcriptionally silence MITF. These include BRN2 (POU3f2), whose expression is mutually exclusive with MITF within tumors (Goodall et al. 2008), and BHLHB2, which is activated under hypoxia (Cheli et al. 2011a). While BRN2-mediated repression of MITF can induce invasion, it is not known whether it may promote invasion by increasing eIF2α phosphorylation. In contrast, low oxygen levels do lead to ER stress and elevated p-eIF2α (Koumenis et al. 2002), which likely contributes to the invasiveness observed under hypoxic conditions (Cheli et al. 2011a).

Previous studies in melanoma have established that, paradoxically, it is rare, stochastically occurring slow-cycling cells in culture that have enhanced tumor–tumor-initiating capacity rather than rapidly proliferating cells

(Roesch et al. 2010; Cheli et al. 2011b). Our results suggest that the greater tumor-initiating capacity of cells following eIF2B inhibition using salubrinal treatment is likely to reflect a combination of four adaptations directly driven by the resulting translation switch: First, reduced nutrient demand owing to a global reduction in translation generates slow-cycling cells that will survive better in low-nutrient-supply environments encountered in vivo than high-demand proliferating cells. Second, changes in cell surface adhesion molecules will enable cells to adhere to niches compatible with survival. Third, ATF4 can promote resistance to anoikis and suppresses oxidative stress (Dey et al. 2015), and coping with oxidative stress is a critical determinant of establishing successful metastases (Piskounova et al. 2015). Fourth, we show that salubrinal or glutamine limitation drives a previously unexplained gene expression program (IPRES) associated with nonresponsiveness to anti-PD-1 immunotherapy, implying that translation reprogramming may engender a state of immune privilege. Thus, cells that leave the primary tumor in response to translation reprogramming are exceptionally well adapted to survive the stresses associated with migration away from the primary tumor.

In summary, our results uncover a previously unsuspected translation reprogramming/ATF4–MITF axis that integrates multiple microenvironmental signals, leading to suppression of MITF and melanoma dedifferentiation, and reveal that it is translation reprogramming upstream of ATF4 that drives gene expression programs associated with therapeutic resistance and metastatic spread.

Materials and methods

Microarray

IGR37 melanoma cells were cultured in DMEM or medium minus glutamine (MEM) for 6, 24, and 72 h. Total RNA was extracted using RNeasy minikits and QIAshredder columns (Qiagen). RNA quality was assessed using a Bioanalyzer (Agilent Technologies). Triplicate samples of each condition were converted into biotin-labeled cRNA, and 30 ng of total RNA was hybridized to a human HT-12 version 4.0 Expression BeadChip and scanned using an IScan (Illumina). The hybridized and washed chips were then scanned using an Illumina iScan scanner using the manufacturer's recommended protocols at the Wellcome Trust Center for Human Genetics at the University of Oxford.

Gene expression analysis

Average probe intensities were determined in Genome Studio (Illumina) and analyzed in a Bioconductor using the limma package (Smyth 2004; Shi et al. 2010). Probe intensities for each array were background-corrected against negative control probes, quantile-normalized against negative and positive control probes, and $\log_2$-transformed. Differential expression analysis was performed by fitting linear models to the data and calculating empirical Bayes moderated *t* statistics. Probes with absolute fold change >2 and Benjamini-Hochberg-adjusted *P*-value of <0.05 were considered differentially expressed. Heat maps were plotted as residuals for the relevant probes, with each probe transformed to give a mean of 0 and variance of 1.

TCGA transcriptomic analysis

Gene expression data (RNA-seq) of TGCA cancer cohorts was accessed through the cBioportal for Cancer Genomics (http://www.cbioportal.org) using the R-based package CGDS-R (Cerami et al. 2012; Gao et al. 2013) and following the TCGA guidelines for the use of TCGA data (http://cancergenome.nih.gov/publications/publicationguidelines). We retrieved individual gene expression values for the genes of interest as normalized RSEM (RNA-seq by expectation maximization) read counts preprocessed through the TCGA/cBioportal projects. RSEM values <1 were set to 1 to avoid negative expression values upon $\log_2$ transformation if necessary. All melanoma samples were ordered by increasing expression values of the averaged GSS. Gene symbols of the gene signatures are provided in the Supplemental Tables. The GSS was established from the glutamine starvation time-course experiments. We included genes that were induced more than twofold at 6 h after the medium change from glutamine-rich DMEM to glutamine-deprived MEM. We decided to use this gene signature from an early time point after glutamine withdrawal, as signatures from latter time points were enriched for secondary effects such as cell cycle arrest and down-regulation of MITF target genes. The moving average expression of individual genes of interest or averaged signatures were calculated using a sample window size of $n = 20$, and trend lines were added to the bar plots. An R-skript for calculating and generating moving average plots of TCGA cancer cohorts implementing TCGA access via cBioportal was provided in our previous study (Riesenberg et al. 2015). Significance of the Spearman rank correlation was determined by an asymptotic Spearman correlation test using the original $\log_2$ expression values and not the moving average values.

GSEA

Gene expression data from untreated or pmel-1 T-cell immunotherapy relapse HCmel3 mouse melanomas were generated in our previous study and deposited in the Gene Expression Omnibus (GEO) archive with the accession number GSE40213. Briefly, raw data were normalized with variance stabilization without background corrections using the vsn2 package of the R-based Bioconductor computing platform. A moderated eBayes *t*-test statistic (limma package) was used to generate a gene-wise rank metric as input for the GSEA preranked gene list algorithm. The java-based GSEA program was downloaded from the GSEA homepage of the Broad Institute (http://www.broadinstitute.org/gsea/index.jsp). GSEA was performed with 10,000 permutations using custom gene sets: the GSS, the Hoek invasive/proliferative signature (Hoek et al. 2006), the Verfaillie invasive/proliferative signature (Verfaillie et al. 2015), and the melanoma cell-derived TNFα response gene set (Riesenberg et al. 2015).

The GSVA program (Hanzelmann et al. 2013) uses a nonparametric unsupervised method of gene set enrichment to estimate the relative enrichment of selected gene sets across all of the samples. We used a gene expression matrix in the form of normalized $\log_2$ TCGA RNA-seq expression values and IPRES gene signatures from Hugo et al. (2016) as inputs, and the output is a gene set enrichment profile in the form of a matrix for each gene set and sample. The salubrinal gene expression signature used represents the 100 most regulated genes in response to 24 h of salubrinal treatment.

Melanoma cell line panels

Raw CEL files of the Broad Institute melanoma portal cell line panel were downloaded from https://www.broadinstitute.org/

software/cprg/?q=node/46. Raw CEL files of the Queensland, Duke, and Zürich melanoma cell lines or short-term culture panels were downloaded from the GEO database using the accession numbers GSE7127, GSE10916, and GSE33728, respectively. Robust multiarray average (RMA; justRMA, R affy package) was used for normalization and $\log_2$ transformation of the gene expression data. GSE7127 and GSE10916 were combined for the analysis, as these panels have been processed on the identical microarray platform (Affymetrix hgu133plus2). The Zürich panel was analyzed separately, as data from functional invasion assays were available for these melanoma short-term cultures. Signature scores were calculated by averaging signals from probes corresponding to the signature genes. Correlations between signatures and invasiveness and *P*-values were determined by Spearman's rank correlation with two-sided alternative testing.

Cell culture

Melanoma cell lines tested for mycoplasma and authenticated by Eurofins-Genomics were cultured in 10% CO_2 at 37°C with 1% penicillin–streptomycin in high-glucose DMEM plus 10% fetal bovine serum (FBS) or MEM with 10% dialyzed FBS (Invitrogen). Where indicated, MEM was supplemented with 42 mg/L 0.4 mM serine, 30 mg/L 0.4 mM glycine, and glutamine at the indicated concentrations. Inducible cell lines were made, luciferase reporters were constructed, and immunofluorescence was performed as described in the Supplemental Material.

Invasion assay

Matrigel invasion assays were performed using an invasion chamber from BD Biocoat. Cells seeded at 2×10^5 cells per insert were cultured overnight in triplicate before treatment with starvation medium or drugs. After 48 h of incubation, cells remaining above the insert membrane were removed by gentle scraping with a sterile cotton swab. Cells that invaded through the Matrigel to the bottom of the insert were fixed in ethanol for 10 min, washed in phosphate-buffered saline (PBS), and stained with Methylene blue. The insert was then washed in PBS and air-dried, and invading cells were counted.

RT-qPCR

Total RNA was extracted from melanoma cells by using the RNeasy minikit (Qiagen). Reverse transcription of 1 µg of RNA was performed according to the manufacturer's instructions using the QuantiTect reverse transcription kit (Qiagen). Primers for human genes were designed using the Primer Blast application from NCBI (see the Supplemental Material). Reactions were done in SYBR Green mix (Go-Taq, Promega) and analyzed using a Corbett Rotor-Gene 6000. Melting curve analyses were carried out to ensure product specificity, and data were analyzed using the $2^{-\Delta\Delta Ct}$ method. Relative mRNA expression levels were normalized to *ACTIN* or *glyceraldehyde3′phosphate dehydrogenase* (*GAPDH*).

Immunofluorescence microscopy

Cells were grown on 100-mm^2 coverslips, fixed in 3% paraformaldehyde, and permeabilized with 0.2% Triton X-100. Coverslips were blocked in 5% BSA in PBS for 20 min and probed with the appropriate antibody (see the Supplemental Material) for 20 min at room temperature. Proteins were detected with fluorochrome-conjugated secondary antibodies (Alexa-488, Alexa-546, and Alexa-647), imaged with an LSM 710 confocal microscope (Carl Zeiss), and processed with Adobe Photoshop CS6 (Adobe Systems). Quantification of the mean fluorescence intensity per cell was performed using ImageJ software.

Inducible cell lines

EcoRI/BamHI small adapters were added to the ends of the ATF4 cDNA, digested, and inserted into pPBhCMV*1-cHA-pA[55] modified to contain mCherry-P2A (self-cleavable peptide) in-frame with the MCS to produce the inducible vector. Cell lines were transfected with FuGENE6 with the mCherry-P2A-ATF4 vector together with CAG-rtTA-IRES-Neo and PiggyBac transposase and selected with 750 µg/mL geneticin for 10 d. Expression of mCherry-P2A-ATF4 was achieved by treating the cells (iATF4) with 100 ng/mL doxycycline. A similar strategy was used to create the 501mel iMITF cell line.

Flow cytometry

Melanoma cells were harvested, washed in PBS, and fixed with 70% ethanol for 1 h at 4°C after indicated treatments. Fixed cells were washed with PBS and incubated with a staining solution containing 50 µg/mL RNase A, 50 µg/mL propidium iodide, and 0.05% Triton X-100 in PBS for 30 min at 37°C. Cells were washed with PBS, and DNA content was analyzed with a FACS Canto flow cytometer (BD Bioscience). Approximately 10,000 cells were used for each analysis. Quantification of cell death was performed by TO-PRO-3 iodide staining of unfixed cells. Cells were treated with the indicated treatments, trypsinized, and harvested in staining solution (PBS, FBS 5%, NaN_3 0.02%). Cells were incubated with a solution of 50 nM TO-PRO-3 for 10 min and analyzed with a FACS Canto flow cytometer (BD Bioscience). TO-PRO-3 DNA intercalator was incorporated by the dead cells, leaving the viable cells unstained. Flow cytometric analyses were performed with FlowJo software.

Lentivirus expression in melanoma cells of eIF2α wild type and S52A

Recombinant lentivirus was made in Phoenix producer cells using the lentiviral vector pCSII-EF-MCS (a kind gift of H. Miyoshi), driving Venus-P2A-eIF2α wild-type or mCherry-P2A-eIF2α S52A expression. Phoenix cells were seeded onto poly-L-lysine-coated plates, and the vectors were cotransfected together with Gag/Pol/Rev- and VSV-containing vectors. The medium was changed after 24 h, and the virus-containing supernatant was harvested 48 and 72 h after transfection and filtered through a 0.45-µm syringe filter. 501mel melanoma cells were infected by incubation with the viral suspension for 48 h. Fresh medium was added and replaced after 24 h. Viral infection typically achieved an efficiency of 100% of cells.

SA-β-gal assay

Cells were seeded in six-well plates (1×10^5 per well), washed twice with PBS, fixed in 2% formaldehyde and 0.2% glutaraldehyde, washed again with PBS, and incubated for 16 h at 37°C (no CO_2) in fresh SA-β-gal buffer (1 mg/mL X-gal, 5 mmol/L potassium ferrocyanide, 5 mmol/L potassium ferricyanide, 2 mmol/L $MgCl_2$ in PBS at pH 6.0). Stained cells were visualized using a Nikon Eclipse TE 2000-S microscope under bright-field, and images were captured with a ProgRes.digital camera using CapturePro software.

Luciferase assay

One kilobase upstream of the ATF4 transcription start site was inserted upstream of the firefly luciferase-coding sequence. Melanoma cells were transfected using FuGENE6 (Promega) with 100 ng of promoter reporter with or without plasmid-expressing activators or empty expression vector. Forty-eight hours after transfection, cells were lysed, and luciferase activity was measured in triplicate using the luciferase reporter kit (Promega) and a Glo-Max Multidetection system.

RNAi

Specific siRNA for MITF (5′-AAAGCAGTACCTTTCTACCAC-3′) and negative control siRNA were obtained from Qiagen and transfected using Lipofectamine 2000 (Invitrogen).

^{35}S-methionine labeling

Cells were plated in 6-cm plates and treated with different starvation media. After 24 h of starvation, cells were washed with PBS, and the medium was replaced with methionine and cysteine-free MEM (plus or minus S, G, or Q) containing 10% dialyzed FBS. Thirty minutes later, 250 µCi/ml [^{35}S]-methionine/cysteine Express protein labeling mix (Perkin Elmer) was added to the medium. After a further 20 min of incubation, cells were placed on ice and washed twice in ice-cold PBS containing 1% cold methionine. Cells were lysed in 500 µL of lysis buffer (10 mM Tris at pH 7.5, 50 mM NaCl, 0.5% NP-40, 0.5% deoxycholate, 0.5% SDS) supplemented with protease inhibitors. The lysate was centrifuged at 13,000 rpm in a benchtop microfuge for 10 min at 4°C, and the supernatant was transferred to a clean 1.5-mL tube. Ten microliters of the lysate was removed, analyzed by SDS-PAGE, and visualized by Coomassie staining and phosphorimager analysis to determinate the protein synthesis rate.

Western blot and antibodies

Cells were lysed in Laemmli buffer in reducing conditions. Whole-cell extracts were subjected to 12% polyacrylamide SDS-PAGE. Proteins were transferred onto nitrocellulose membranes (Amersham Biosciences). Membranes were blocked with 5% nonfat milk (or 5% BSA for blots using anti-phospho-specific antibodies) in PBS containing 0.1% Tween 20 and probed with the appropriate primary antibodies (see the Supplemental Material) overnight at 4°C. Proteins were detected using anti-mouse, anti-rabbit, or anti-goat immunoglobulin coupled to horseradish peroxidase (Bio-Rad and Santa Cruz Biotechnology) and visualized with an ECL detection kit (Amersham Biosciences)

Tumorigenesis assays

Specific pathogen-free 8-wk-old female C57/BL6 mice purchased from Harlan Envigo laboratories were maintained in University of Oxford facilities in accordance with UK Home Office regulations, monitored daily, and sacrificed at or before the first sign of irregular behavior, appearance, or distress. B16F10 cells were harvested using 0.25% trypsin and 0.02% EDTA and washed twice with PBS. Only cell suspensions with >90% viability were used for injections. Tumor cells (2.0×10^5 cells) in 100 µL of PBS were injected into the lateral tail veins. Mice were sacrificed at the defined days after injections, and lung tumor colonies were counted under a dissecting microscope.

Data

Gene array data were deposited in NCBI GEO under accession numbers GSE77655 (glutamine limitation) and GSE86806 (salubrinal).

Acknowledgments

The original Piggybac vectors were provided by Kazuhiro Murakami (RIKEN, Kobe, Japan), and the FLO8 plasmid was provided by Gerry Fink (Whitehead Institute); human melanoma data were provided by TCGA (http://cancergenome.nih.gov). This work was funded by the Ludwig Institute for Cancer Research (C.R.G., L.S.-d.-C., P.F., R.S., and X.L.), National Institutes of Health grant PO1 CA128814-06A1 (to P.F.), the Fundación Seneca, the Fundación de la Associación Española Contra el Cáncer (FAECC), the Ministerio de Economia y Competitividad (MINECO; cofinancing with Fondo Europeo de Desarrollo Regional; SAF2013-48375-C2-1-R to L.S.-d.-C.), the Deutsche Forschungsgemeinschaft (HO4281/2-1 to M.E. and M.H.), the Medical Research Council (A.E.W.), the Oxford Biomedical Research Centre (J.C. and R.L.), the Biotechnology and Biological Sciences Research Council (grant BB/M006565/1 to G.P. and C. J.K.), the Wellcome Trust (WT098519MA to M.J.D.), the National Cancer Institute (CA128814 to Z.A.R.), Cancer Research UK (CRUK; grant number C5255/A18085 through the CRUK Oxford Centre to C.R.G., and C5255/A15935 to F.M.B.), and the Oxford National Institute for Health Research Biomedical Research Centre (M.M.). L.S-d-C., P.F., and C.R.G. conceived the project and designed and interpreted experiments. P.F., L.S-d-C., M.E., A.K., and C.J.K., performed experiments with assistance from R.L. and R.F. R.S. and J.C. undertook bioinformatics analysis. M.J.D., X.L., T. T., M.M., F.M.B., A.E.W., G.P., Z.A.R., T.S.-S., M.H., and C.R. G. provided resources and supervision. C.R.G., P.F., L.S.-d-C., and M.H. wrote the manuscript.

References

Augustine CK, Yoo JS, Potti A, Yoshimoto Y, Zipfel PA, Friedman HS, Nevins JR, Ali-Osman F, Tyler DS. 2009. Genomic and molecular profiling predicts response to temozolomide in melanoma. *Clin Cancer Res* **15:** 502–510.

Baenke F, Chaneton B, Smith M, Van Den Broek N, Hogan K, Tang H, Viros A, Martin M, Galbraith L, Girotti MR, et al. 2016. Resistance to BRAF inhibitors induces glutamine dependency in melanoma cells. *Mol Oncol* **10:** 73–84.

Bertolotto C, Bille K, Ortonne J-P, Ballotti R. 1996. Regulation of tyrosinase gene expression by cAMP in B16 melanoma cells involves two CATGTG motifs surrounding the TATA box: implication of the microphthalmia gene product. *J Cell Sci* **134:** 747–755.

Boyce M, Bryant KF, Jousse C, Long K, Harding HP, Scheuner D, Kaufman RJ, Ma D, Coen DM, Ron D, et al. 2005. A selective inhibitor of eIF2α dephosphorylation protects cells from ER stress. *Science* **307:** 935–939.

Caramel J, Papadogeorgakis E, Hill L, Browne GJ, Richard G, Wierinckx A, Saldanha G, Osborne J, Hutchinson P, Tse G, et al. 2013. A switch in the expression of embryonic EMT-inducers drives the development of malignant melanoma. *Cancer Cell* **24:** 466–480.

Carreira S, Goodall J, Denat L, Rodriguez M, Nuciforo P, Hoek KS, Testori A, Larue L, Goding CR. 2006. Mitf regulation of Dia1 controls melanoma proliferation and invasiveness. *Genes Dev* **20:** 3426–3439.

Cerami E, Gao J, Dogrusoz U, Gross BE, Sumer SO, Aksoy BA, Jacobsen A, Byrne CJ, Heuer ML, Larsson E, et al. 2012. The cBio cancer genomics portal: an open platform for exploring multidimensional cancer genomics data. *Cancer Discov* **2:** 401–404.

Cerezo M, Lehraiki A, Millet A, Rouaud F, Plaisant M, Jaune E, Botton T, Ronco C, Abbe P, Amdouni H, et al. 2016. Compounds triggering ER stress exert anti-melanoma effects and overcome BRAF inhibitor resistance. *Cancer Cell* **29:** 805–819.

Cheli Y, Ohanna M, Ballotti R, Bertolotto C. 2010. Fifteen-year quest for microphthalmia-associated transcription factor target genes. *Pigment Cell Melanoma Res* **23:** 27–40.

Cheli Y, Giuliano S, Fenouille N, Allegra M, Hofman V, Hofman P, Bahadoran P, Lacour JP, Tartare-Deckert S, Bertolotto C, et al. 2011a. Hypoxia and MITF control metastatic behaviour in mouse and human melanoma cells. *Oncogene* **31:** 2461–2470.

Cheli Y, Guiliano S, Botton T, Rocchi S, Hofman V, Hofman P, Bahadoran P, Bertolotto C, Ballotti R. 2011b. Mitf is the key molecular switch between mouse or human melanoma initiating cells and their differentiated progeny. *Oncogene* **30:** 2307–2318.

De Gassart A, Bujisic B, Zaffalon L, Decosterd LA, Di Micco A, Frera G, Tallant R, Martinon F. 2016. An inhibitor of HIV-1 protease modulates constitutive eIF2α dephosphorylation to trigger a specific integrated stress response. *Proc Natl Acad Sci* **113:** E117–E126.

Dey S, Sayers CM, Verginadis II, Lehman SL, Cheng Y, Cerniglia GJ, Tuttle SW, Feldman MD, Zhang PJ, Fuchs SY, et al. 2015. ATF4-dependent induction of heme oxygenase 1 prevents anoikis and promotes metastasis. *J Clin Invest* **125:** 2592–2608.

Du J, Widlund HR, Horstmann MA, Ramaswamy S, Ross K, Huber WE, Nishimura EK, Golub TR, Fisher DE. 2004. Critical role of CDK2 for melanoma growth linked to its melanocyte-specific transcriptional regulation by MITF. *Cancer Cell* **6:** 565–576.

Dugo M, Nicolini G, Tragni G, Bersani I, Tomassetti A, Colonna V, Del Vecchio M, De Braud F, Canevari S, Anichini A, et al. 2015. A melanoma subtype with intrinsic resistance to BRAF inhibition identified by receptor tyrosine kinases gene-driven classification. *Oncotarget* **6:** 5118–5133.

Elkabets M, Pazarentzos E, Juric D, Sheng Q, Pelossof RA, Brook S, Benzaken AO, Rodon J, Morse N, Yan JJ, et al. 2015. AXL mediates resistance to PI3Kα inhibition by activating the EGFR/PKC/mTOR axis in head and neck and esophageal squamous cell carcinomas. *Cancer Cell* **27:** 533–546.

Feng Y-XX, Sokol ES, Del Vecchio CA, Sanduja S, Claessen JH, Proia TA, Jin DX, Reinhardt F, Ploegh HL, Wang Q, et al. 2014. Epithelial-to-mesenchymal transition activates PERK–eIF2α and sensitizes cells to endoplasmic reticulum stress. *Cancer Discov* **4:** 702–715.

Gao J, Aksoy BA, Dogrusoz U, Dresdner G, Gross B, Sumer SO, Sun Y, Jacobsen A, Sinha R, Larsson E, et al. 2013. Integrative analysis of complex cancer genomics and clinical profiles using the cBioPortal. *Science Signaling* **6:** pl1.

Garraway LA, Widlund HR, Rubin MA, Getz G, Berger AJ, Ramaswamy S, Beroukhim R, Milner DA, Granter SR, Du J, et al. 2005. Integrative genomic analyses identify MITF as a lineage survival oncogene amplified in malignant melanoma. *Nature* **436:** 117–122.

Gimeno CJ, Ljungdahl PO, Styles CA, Fink GR. 1992. Unipolar cell divisions in the yeast *S. cerevisiae* lead to filamentous growth: regulation by starvation and RAS. *Cell* **68:** 1077–1090.

Giuliano S, Cheli Y, Ohanna M, Bonet C, Beuret L, Bille K, Loubat A, Hofman V, Hofman P, Ponzio G, et al. 2010. Microphthalmia-associated transcription factor controls the DNA damage response and a lineage-specific senescence program in melanomas. *Cancer Res* **70:** 3813–3822.

Goodall J, Carreira S, Denat L, Kobi D, Davidson I, Nuciforo P, Sturm RA, Larue L, Goding CR. 2008. Brn-2 represses microphthalmia-associated transcription factor expression and marks a distinct subpopulation of microphthalmia-associated transcription factor-negative melanoma cells. *Cancer Res* **68:** 7788–7794.

Gray-Schopfer VC, Cheong SC, Chong H, Chow J, Moss T, Abdel-Malek ZA, Marais R, Wynford-Thomas D, Bennett DC. 2006. Cellular senescence in naevi and immortalisation in melanoma: a role for p16? *British J Cancer* **95:** 496–505.

Han J, Back SH, Hur J, Lin YH, Gildersleeve R, Shan J, Yuan CL, Krokowski D, Wang S, Hatzoglou M, et al. 2013. ER-stress-induced transcriptional regulation increases protein synthesis leading to cell death. *Nat Cell Biol* **15:** 481–490.

Hanzelmann S, Castelo R, Guinney J. 2013. GSVA: gene set variation analysis for microarray and RNA-seq data. *BMC Bioinformatics* **14:** 7.

Harding HP, Zhang Y, Zeng H, Novoa I, Lu PD, Calfon M, Sadri N, Yun C, Popko B, Paules R, et al. 2003. An integrated stress response regulates amino acid metabolism and resistance to oxidative stress. *Mol Cell* **11:** 619–633.

Hemesath TJ, Price ER, Takemoto C, Badalian T, Fisher DE. 1998. MAP kinase links the transcription factor Microphthalmia to c-Kit signalling in melanocytes. *Nature* **391:** 298–301.

Hernandez-Davies JE, Tran TQ, Reid MA, Rosales KR, Lowman XH, Pan M, Moriceau G, Yang Y, Wu J, Lo RS, et al. 2015. Vemurafenib resistance reprograms melanoma cells towards glutamine dependence. *J Transl Med* **13:** 210.

Hodgkinson CA, Moore KJ, Nakayama A, Steingrimsson E, Copeland NG, Jenkins NA, Arnheiter H. 1993. Mutations at the mouse *microphthalmia* locus are associated with defects in a gene encoding a novel basic-helix-loop-helix-zipper protein. *Cell* **74:** 395–404.

Hoek KS, Schlegel NC, Brafford P, Sucker A, Ugurel S, Kumar R, Weber BL, Nathanson KL, Phillips DJ, Herlyn M, et al. 2006. Metastatic potential of melanomas defined by specific gene expression profiles with no BRAF signature. *Pigment Cell Res* **19:** 290–302.

Hugo W, Zaretsky JM, Sun L, Song C, Moreno BH, Hu-Lieskovan S, Berent-Maoz B, Pang J, Chmielowski B, Cherry G, et al. 2016. Genomic and transcriptomic features of response to anti-PD-1 therapy in metastatic melanoma. *Cell* **165:** 35–44.

Jeong Y, Du R, Zhu X, Yin S, Wang J, Cui H, Cao W, Lowenstein CJ. 2014. Histone deacetylase isoforms regulate innate immune responses by deacetylating mitogen-activated protein kinase phosphatase-1. *J Leukoc Biol* **95:** 651–659.

Johannessen CM, Johnson LA, Piccioni F, Townes A, Frederick DT, Donahue MK, Narayan R, Flaherty KT, Wargo JA, Root DE, et al. 2013. A melanocyte lineage program confers resistance to MAP kinase pathway inhibition. *Nature* **504:** 138–142.

Kamphorst JJ, Nofal M, Commisso C, Hackett SR, Lu W, Grabocka E, Vander Heiden MG, Miller G, Drebin JA, Bar-Sagi D, et al. 2015. Human pancreatic cancer tumors are nutrient poor and tumor cells actively scavenge extracellular protein. *Cancer Res* **75:** 544–553.

Konieczkowski DJ, Johannessen CM, Abudayyeh O, Kim JW, Cooper ZA, Piris A, Frederick DT, Barzily-Rokni M, Straussman R, Haq R, et al. 2014. A melanoma cell state distinction

influences sensitivity to MAPK pathway inhibitors. *Cancer Discov* **4:** 816–827.

Koumenis C, Naczki C, Koritzinsky M, Rastani S, Diehl A, Sonenberg N, Koromilas A, Wouters BG. 2002. Regulation of protein synthesis by hypoxia via activation of the endoplasmic reticulum kinase PERK and phosphorylation of the translation initiation factor eIF2α. *Mol Cell Biol* **22:** 7405–7416.

Landsberg J, Kohlmeyer J, Renn M, Bald T, Rogava M, Cron M, Fatho M, Lennerz V, Wolfel T, Holzel M, et al. 2012. Melanomas resist T-cell therapy through inflammation-induced reversible dedifferentiation. *Nature* **490:** 412–416.

Lin WM, Baker AC, Beroukhim R, Winckler W, Feng W, Marmion JM, Laine E, Greulich H, Tseng H, Gates C, et al. 2008. Modeling genomic diversity and tumor dependency in malignant melanoma. *Cancer Res* **68:** 664–673.

Ma H, Groth RD, Cohen SM, Emery JF, Li B, Hoedt E, Zhang G, Neubert TA, Tsien RW. 2014. γCaMKII shuttles Ca^{2+}/CaM to the nucleus to trigger CREB phosphorylation and gene expression. *Cell* **159:** 281–294.

Michaloglou C, Vredeveld LC, Soengas MS, Denoyelle C, Kuilman T, van der Horst CM, Majoor DM, Shay JW, Mooi WJ, Peeper DS. 2005. BRAFE600-associated senescence-like cell cycle arrest of human naevi. *Nature* **436:** 720–724.

Muller J, Krijgsman O, Tsoi J, Robert L, Hugo W, Song C, Kong X, Possik PA, Cornelissen-Steijger PD, Foppen MH, et al. 2014. Low MITF/AXL ratio predicts early resistance to multiple targeted drugs in melanoma. *Nat Commun* **5:** 5712.

Ostyn P, El Machhour R, Begard S, Kotecki N, Vandomme J, Flamenco P, Segard P, Masselot B, Formstecher P, Touil Y, et al. 2014. Transient TNF regulates the self-renewing capacity of stem-like label-retaining cells in sphere and skin equivalent models of melanoma. *Cell Commun Signal* **12:** 52.

Pan M, Reid MA, Lowman XH, Kulkarni RP, Tran TQ, Liu X, Yang Y, Hernandez-Davies JE, Rosales KK, Li H, et al. 2016. Regional glutamine deficiency in tumours promotes dedifferentiation through inhibition of histone demethylation. *Nat Cell Biol* **18:** 1090–1101.

Piskounova E, Agathocleous M, Murphy MM, Hu Z, Huddlestun SE, Zhao Z, Leitch AM, Johnson TM, DeBerardinis RJ, Morrison SJ. 2015. Oxidative stress inhibits distant metastasis by human melanoma cells. *Nature* **527:** 186–191.

Price ER, Ding H-F, Badalian T, Bhattacharya S, Takemoto C, Yao T-P, Hemesath TJ, Fisher DE. 1998. Lineage-specific signalling in melanocytes: c-Kit stimulation recruits p300/CBP to Microphthalmia. *J Biol Chem* **273:** 17983–17986.

Riesenberg S, Groetchen A, Siddaway R, Bald T, Reinhardt J, Smorra D, Kohlmeyer J, Renn M, Phung B, Aymans P, et al. 2015. MITF and c-Jun antagonism interconnects melanoma dedifferentiation with pro-inflammatory cytokine responsiveness and myeloid cell recruitment. *Nat Commun* **6:** 8755.

Roberts E, Tanaka KK, Tanaka T, Simonsen DG. 1956. Free amino acids in growing and regressing acites cell tumors: host resistance and chemical agents. *Cancer Res* **16:** 970–978.

Roesch A, Fukunaga-Kalabis M, Schmidt EC, Zabierowski SE, Brafford PA, Vultur A, Basu D, Gimotty P, Vogt T, Herlyn M. 2010. A temporarily distinct subpopulation of slow-cycling melanoma cells is required for continuous tumor growth. *Cell* **141:** 583–594.

Saez-Ayala M, Montenegro MF, Sanchez-Del-Campo L, Fernandez-Perez MP, Chazarra S, Freter R, Middleton M, Pinero-Madrona A, Cabezas-Herrera J, Goding CR, et al. 2013. Directed phenotype switching as an effective antimelanoma strategy. *Cancer Cell* **24:** 105–119.

Shi L, Campbell G, Jones WD, Campagne F, Wen Z, Walker SJ, Su Z, Chu TM, Goodsaid FM, Pusztai L, et al. 2010. The MicroArray Quality Control (MAQC)-II study of common practices for the development and validation of microarray-based predictive models. *Nat Biotechnol* **28:** 827–838.

Sidrauski C, Tsai JC, Kampmann M, Hearn BR, Vedantham P, Jaishankar P, Sokabe M, Mendez AS, Newton BW, Tang EL, et al. 2015. Pharmacological dimerization and activation of the exchange factor eIF2B antagonizes the integrated stress response. *Elife* **4:** e07314.

Smith MP, Sanchez-Laorden B, O'Brien K, Brunton H, Ferguson J, Young H, Dhomen N, Flaherty KT, Frederick DT, Cooper ZA, et al. 2014. The immune microenvironment confers resistance to MAPK pathway inhibitors through macrophage-derived TNFα. *Cancer Discov* **4:** 1214–1229.

Smith MP, Brunton H, Rowling EJ, Ferguson J, Arozarena I, Miskolczi Z, Lee JL, Girotti MR, Marais R, Levesque MP, et al. 2016. Inhibiting drivers of non-mutational drug tolerance is a salvage strategy for targeted melanoma therapy. *Cancer Cell* **29:** 270–284.

Smyth GK. 2004. Linear models and empirical bayes methods for assessing differential expression in microarray experiments. *Stat Appl Genet Mol Biol* **3:** 1–25.

Strub T, Giuliano S, Ye T, Bonet C, Keime C, Kobi D, Le Gras S, Cormont M, Ballotti R, Bertolotto C, et al. 2011. Essential role of microphthalmia transcription factor for DNA replication, mitosis and genomic stability in melanoma. *Oncogene* **30:** 2319–2332.

Tirosh I, Izar B, Prakadan SM, Wadsworth MH, Treacy D, Trombetta JJ, Rotem A, Rodman C, Lian C, Murphy G, et al. 2016. Dissecting the multicellular ecosystem of metastatic melanoma by single-cell RNA-seq. *Science* **352:** 189–196.

Verfaillie A, Imrichova H, Atak ZK, Dewaele M, Rambow F, Hulselmans G, Christiaens V, Svetlichnyy D, Luciani F, Van den Mooter L, et al. 2015. Decoding the regulatory landscape of melanoma reveals TEADS as regulators of the invasive cell state. *Nat Commun* **6:** 6683.

Wang Q, Beaumont KA, Otte NJ, Font J, Bailey CG, van Geldermalsen M, Sharp DM, Tiffen JC, Ryan RM, Jormakka M, et al. 2014. Targeting glutamine transport to suppress melanoma cell growth. *Int J Cancer* **135:** 1060–1071.

Widmer DS, Cheng PF, Eichhoff OM, Belloni BC, Zipser MC, Schlegel NC, Javelaud D, Mauviel A, Dummer R, Hoek KS. 2012. Systematic classification of melanoma cells by phenotype-specific gene expression mapping. *Pigment Cell Melanoma Res* **25:** 343–353.

Wise DR, Thompson CB. 2010. Glutamine addiction: a new therapeutic target in cancer. *Trends Biochem Sci* **35:** 427–433.

Wolchok JD, Kluger H, Callahan MK, Postow MA, Rizvi NA, Lesokhin AM, Segal NH, Ariyan CE, Gordon R-AA, Reed K, et al. 2013. Nivolumab plus ipilimumab in advanced melanoma. *N Engl J Med* **369:** 122–133.

Translation reprogramming is an evolutionarily conserved driver of phenotypic plasticity and therapeutic resistance in melanoma

Paola Falletta, Luis Sanchez-del-Campo, Jagat Chauhan, et al.

Genes Dev. 2017, **31:** originally published online January 17, 2017
Access the most recent version at doi:10.1101/gad.290940.116